Modelling evaporation processes in soils from the Huasco salt flat basin, Chile

M.F. Hernandez Lopez, Isabelle Braud, J. Gironas, F. Suarez, J.F. Munoz

Author-produced version of the article published in Hydrological Processes (2016), 30 25: 4704-4719
The original publication is available at http://onlinelibrary.wiley.com doi:10.1002/hyp.10987

Modeling evaporation processes in soils from the Huasco salt flat basin, Chile

María Fernanda Hernández-López[1,2], Isabelle Braud[3] Jorge Gironás[2,4,5], Francisco Suárez[2,4,*], José Francisco Muñoz[2]

[1] AMEC, Environment & Infrastructure, Av. Apoquindo 3846 / Las Condes, Santiago, Chile.

[2] Departamento de Ingeniería Hidráulica y Ambiental, Pontificia Universidad Católica de Chile, Av. Vicuña Mackenna 4860, Santiago, Chile. Casilla 306, Correo 22, Santiago, Chile.

[3] Irstea, UR HHLY, 5 Rue de la Doua, CS 70077, 69626 Villeurbanne Cedex, France.

[4] Centro de Desarrollo Urbano Sustentable (CEDEUS), CONICYT/FONDAP/15110020, Santiago, RM, Chile.

[5] Centro de Investigación para la Gestión Integrada de Desastres Naturales (CIGIDEN), CONICYT/FONDAP/15110017, Santiago, RM, Chile.

[*] Corresponding author: fsuarez@ing.puc.cl.

Manuscript resubmitted: July 2016

Author-produced version of the article published in Hydrological Processes (2016), 30 25: 4704-4719
The original publication is available at http://onlinelibrary.wiley.com doi:10.1002/hyp.10987

ABSTRACT

The need to understand and simulate hydrological phenomena and their interactions, and the impact of anthropogenic and climate changes on natural environments have promoted the study of evaporation from bare soils in arid climates. In closed Altiplano basins, such as those encountered in arid and hyper arid basins in northern Chile, evaporation from shallow groundwater is the main source of aquifer depletion and thus, its study is crucial for water resources management. The objective of this work is to understand the mechanisms of evaporation in saline soils with shallow water tables, in order to better quantify evaporation fluxes and improve our understanding of the water balance in these regions. To achieve this objective, a model that couples fluid flow with heat transfer was developed and calibrated using column experiments with saline soils from the Huasco salt flat basin, Chile. The model enables determination of both liquid and water vapor fluxes, as well as the location of the evaporation front. Experimental results showed that salt transport inside the soil profile modified the water retention curve, highlighting the importance of including salt transport when modeling the evaporation processes in these soils. Indeed, model simulations only agreed with the experimental data when the effect of salt transport on water retention curves was taken into account. Model results also showed that the evaporation front is closer to the soil surface as the water table depth reduces. Therefore, the model allows determining the groundwater level depth that results in disconnection of liquid fluxes in the vadose zone. A sensitivity analysis allowed understanding the effect of water-flux enhancements mechanisms on soil evaporation. The results presented in this study are important as they allow quantifying the evaporation that occurs in bare soils from Altiplano basins, which is typically the main water discharge in these closed basins.

Keywords: Soil evaporation, Altiplano basins, saline soil column, vapor flow, SiSPAT

Author-produced version of the article published in Hydrological Processes (2016), 30 25: 4704-4719
The original publication is available at http://onlinelibrary.wiley.com doi:10.1002/hyp.10987

1. Introduction

The need to understand and simulate hydrological phenomena and their interactions, and the impact of anthropogenic and climate changes on natural environments have promoted the study of evaporation from bare soils in arid climates (Alazard et al., 2015). However, current knowledge of evaporation remains incomplete because the complex and strongly coupled interaction of transport mechanisms (phase change, capillary flow, film flow, vapor diffusion), soil properties (hydrodynamic and thermal), and atmospheric forcings (air temperature, relative humidity, radiation, atmospheric stability) are not well understood (Trautz et al., 2015). In closed Altiplano basins such as those encountered in arid and hyper arid basins in the northern Chile, evaporation is the main source of aquifer depletion, and thus its study is crucial for water resources management. Understanding evaporation is also important for the study of sensitive soil systems such as wetlands (de la Fuente and Niño, 2010; Johnson et al., 2010). Nonetheless, understanding the evaporation processes in these environments is complex because evaporation occurs under non-isothermal conditions, where water can be mobilized as liquid water or water vapor (Nassar and Horton, 1989; Grifoll et al., 2005; Hernández-López, 2014). In addition, quantifying evaporation in Altiplano basins is difficult due to the harsh conditions, the spatial variability of the evaporation rates, and also due to the difficulty in accessing this region (Kampf et al., 2005; Johnson et al., 2010).

Many studies have been carried out using laboratory soil columns to improve the knowledge on the evaporation mechanisms, focusing on the combined transport of water, heat and solutes (Nassar and Horton, 1989; Cahill and Parlange, 1998; Konukcu et al., 2004; Braud et

al., 2005b; 2009a; Gran et al., 2011; Nachshon et al., 2011; Schulz et al., 2015). These studies have been performed in homogeneous soils of sand or silt under saturated conditions at the beginning of the experiments, and have used saline solutions or deionized water. These investigations have enabled the calibration and validation of numerical models to solve the coupled equations of liquid water, water vapor, heat and solute flows, which can be used as predictive tools to quantify evaporation fluxes in arid regions (Boulet et al., 1997; Grifoll et al., 2005; Braud et al., 2009b; Saito et al., 2006; Novak, 2010). Nonetheless, few studies have tried to understand the evaporation processes in a homogeneous natural saline medium from Altiplano basins (Johnson et al., 2010; Hernández-López et al., 2014). Moreover, Lictevout et al. (2013), who performed an extensive assessment of the water resources in the north of Chile, highlights that the main problem in the Altiplanic closed basins is the lack of evaporation data. Although studies that involve field data collection have been carried out in these regions, e.g., see Johnson et al. (2010), numerical modelling has not been used to quantify the different evaporation processes that occur in the soils from these environments. In a recent study, Hernández-López et al. (2014) measured the temporal and spatial evolution of soil water content, electrical conductivity and temperature under different groundwater levels in a laboratory column filled with natural saline soil from the Huasco salt flats basin, Chile. They estimated the thermal and isothermal liquid and vapor fluxes and tried to determine the location of the evaporation front, which could not be precisely determined due to their sensors' poor spatial resolution. Nonetheless, these experiments provided a valuable data set that can be used to better understand evaporation processes in saline soils with shallow water tables using numerical modelling.

Author-produced version of the article published in Hydrological Processes (2016), 30 25: 4704-4719
The original publication is available at http://onlinelibrary.wiley.com doi:10.1002/hyp.10987

The objective of this work is to complement the measurements performed by Hernández-López et al. (2014) by conducting a modeling study that can improve the understanding of evaporation processes from bare soils in the Chilean Altiplano basins. The specific objectives of this study are to: (1) develop and calibrate a numerical model that can represent the soil water content and thermal profiles, as well as the evaporation fluxes; (2) simulate liquid water and water vapor fluxes to locate the evaporation front; and (3) perform a sensitivity analysis on the calibrated parameters to ensure their validity based on physical constrains. To achieve these objectives, we used the bare soil version of the SiSPAT (Simple Soil Plant Atmosphere Transfer) model (Braud et al., 1995) and optimized the soil hydrodynamic and thermal properties to adequately represent the experiments reported by Hernández-López et al. (2014). Different water fluxes were analyzed in detail using the optimized model results for two water table levels, and the location of the evaporation front was found. A sensitivity analysis was carried out to better understand the uncertainty that calibration parameters (e.g., tortuosity, enhancement factor) have on evaporation, and finally a discussion of the limitations of our approach is presented.

2 Materials and Methods

2.1 Soil hydraulic properties

In this study, we utilized the soil collected by Hernández-López et al. (2014) from the Huasco salt flat basin, Chile. This soil had 95% sand, 4% silt, 1% clay, an *in-situ* dry bulk density of 1.55 g cm^{-3}, and a soil bulk electrical conductivity of 8.1 dS m^{-1} (measured at a soil water content of ~0.07 m^3 m^{-3}). The soil's water retention curve was obtained experimentally using a 5-bar pressure plate extractor (1660, Soilmoisture Equipment Corp., Santa Barbara, CA). The van

Author-produced version of the article published in Hydrological Processes (2016), 30 25: 4704-4719
The original publication is available at http://onlinelibrary.wiley.com doi:10.1002/hyp.10987

Genuchten model (1980) was fitted to the experimental measurements to estimate the parameters of the water retention curve:

$$\theta(h) = \theta_r + \frac{\theta_s - \theta_r}{\left[1 + (\alpha h)^n\right]^m} \quad (1)$$

where θ (m^3 m^{-3}) is the volumetric water content; θ_r and θ_s (m^3 m^{-3}) are the residual and saturated water contents, respectively; α (m^{-1}) is the inverse of the air-entry pressure; h (m) is the soil water suction or negative pressure expressed as an equivalent water column; and n and m (-) are empirical parameters. In the following, we use the Mualem hypothesis (i.e., m = 1-1/n).

The saturated hydraulic conductivity, K_s (m s^{-1}), was measured using a constant head permeameter (Soil Measurement System, Tucson, AZ), and the unsaturated hydraulic conductivity was determined using the Brooks-Corey-Burdine model (Brooks and Corey, 1964):

$$K(\theta) = K_S \left(\frac{\theta}{\theta_S}\right)^{\beta} \quad (2)$$

where $K(\theta)$ (m s^{-1}) is the hydraulic conductivity at a volumetric water content of θ, and β (-) is an empirical coefficient.

2.2 Evaporation experiments

Quasi steady state soil evaporation experiments were conducted in a laboratory with controlled environmental conditions (ambient temperature of 22 ± 2.5°C and relative humidity between 25% and 58%). An unaltered dry soil sample collected from the Huasco salt flat basin was transported in layers to the laboratory and packed homogeneously in an insulated acrylic

Author-produced version of the article published in Hydrological Processes (2016), 30 25: 4704-4719
The original publication is available at http://onlinelibrary.wiley.com doi:10.1002/hyp.10987

column of 0.35 m internal diameter and 1.20 m height. The packing reproduced the in-situ dry bulk density.

The bottom of the soil column was connected to an external reservoir, which fixed the water table level within the column. Temperature (T) was measured in the soil profile using thermistors (107-L, Campbell Sci., Logan, UT). Soil water content (θ) and electrical conductivity (σ) were measured using time domain reflectometry (TDR) probes (CS645, Campbell Sci., Logan, UT). The accuracy and precision in the measurement of the soil water content were 0.5% and 0.05%, respectively. The accuracy in the electrical conductivity measurements was ~1%. Temperature and TDR probes were installed at nine depths in the soil profile spaced equally between 5 and 45 cm depth (measured from the soil surface). These data were collected using a datalogger (CR1000, Campbell Sci., Logan, UT).

In the first experiment, the external reservoir fixed the water level at 0.75 m (below the soil surface). The evaporation experiments were carried out using tap water and thus the source of salinity was the soil itself. Evaporation was driven by an infrared lamp (General Electric IR 150 W) located 0.30 m above the soil surface and enhanced using a fan that simulated wind speeds of 0.2 m s^{-1}. The infrared lamp was on from 8:00 to 18:00 hours to simulate the diurnal cycle of solar radiation. Air temperature and relative humidity measurements were recorded in the laboratory and at the surface of the column with two shielded sensors (HMP75, Vaisala, Helsinki, Finland) at 15-min intervals. Daily evaporation rates were estimated with a precision of 0.7 mm day^{-1} from the water level fluctuations in the external reservoir. The profiles of T, θ, and σ were monitored at 5-min intervals, and the evaporated water was replenished daily in the

Author-produced version of the article published in Hydrological Processes (2016), 30 25: 4704-4719
The original publication is available at http://onlinelibrary.wiley.com doi:10.1002/hyp.10987

147 external reservoir to maintain a fixed water level. When the previous variables varied in less than
148 1%, it was assumed that steady state was reached (typically after ~20 days). This state was used
149 to model the evaporation process within the soil column (described below). Then, the water level
150 was raised to a depth of 0.40 m and the experiment was repeated. More details about these
151 experiments are presented in Hernández-López et al. (2014), in which evaporation rates vs. water
152 table depth observations in the laboratory are successfully compared to lysimeters and in-situ
153 chamber measurements in the Huasco salt flat basin.

154 ## *2.3 Description of the numerical model*

155 ### *2.3.1 Water flow and heat transport equations*

156 To represent the hydrodynamics in the evaporation experiments, we adapted the SiSPAT
157 model (Braud et al., 1995) to the laboratory conditions. SiSPAT simulates the one-dimensional
158 heat and water transfer in the soil-plant-atmosphere system by coupling the liquid and water
159 vapor flow equations based on the approach of Philip and de Vries (1957), modified by Milly
160 (1984). The modified SiSPAT model is divided into three modules: soil, atmosphere, and soil-
161 atmosphere interface. In the soil module, water flow and heat transport are described as a coupled
162 system of two mass and heat transfer equations that predict temperature and soil water suction
163 fields:

164 $$C_h \frac{\partial h}{\partial t} = \frac{\partial}{\partial z}\left(D_{mh} \frac{\partial h}{\partial z} + D_{mT} \frac{\partial T}{\partial z} - K(h) \right) \quad (3)$$

165 $$C_T \frac{\partial T}{\partial t} = \frac{\partial}{\partial z}\left(D_{ch} \frac{\partial h}{\partial z} + \lambda \frac{\partial T}{\partial z} \right) \quad (4)$$

Author-produced version of the article published in Hydrological Processes (2016), 30 25: 4704-4719
The original publication is available at http://onlinelibrary.wiley.com doi:10.1002/hyp.10987

where T is the soil temperature (K), C_h (m^{-1}) and C_T (J m^{-3} K^{-1}) are the capillary capacity and volumetric heat capacity, respectively; t (s) is time; and z (m) is the spatial coordinate oriented downward. The transport coefficients are the isothermal hydraulic conductivity $D_{mh} = K + D_{vh} / \rho_w$ (m s^{-1}), the thermal vapor hydraulic conductivity $D_{mT} = D_{vT} / \rho_w$ (m^2 K^{-1} s^{-1}), the isothermal vapor hydraulic conductivity $D_{ch} = L_v D_{vh}$ (m s^{-1}), and the apparent thermal conductivity λ (W m^{-1} K^{-1}). *K(h)* (m s^{-1}) is the unsaturated hydraulic conductivity of the liquid phase as a function of water suction, D_{vh} (m^2 s^{-1}) is the isothermal vapor diffusivity, D_{vT} (m^2 s^{-1}) is the thermal vapor diffusivity, ρ_w (kg m^{-3}) is the water density, and L_v (J kg^{-1}) is the latent heat of vaporization. All these coefficients can be expressed as function of soil water content and/or temperature, as shown in Table 1. Note that D_{vh} and D_{vT} are function of the tortuosity factor, τ_a, and the enhancement factor, η, respectively, as shown in Table 1. The description of the tortuosity and enhancement factors is provided with more details in section 2.4.

2.3.2 Model parameters and initial and boundary conditions

In the model, the soil column was first discretized using only one horizon and a variable grid spacing with a finer resolution close to the top and bottom interfaces (minimum and maximum layer thickness of 0.001 and 0.005-m respectively) to simulate a vertically homogeneous soil. Then, different horizons were adopted to simulate spatial heterogeneity (described below). This approach required considering variable thicknesses with finer resolutions close to the interfaces between horizons. In this last case, the minimum and maximum layer thicknesses were 0.001 m and 0.005 m respectively. Table 2 presents the model parameters, and the chosen initial and boundary conditions used to represent the evaporation experiments for the

Author-produced version of the article published in Hydrological Processes (2016), 30 25: 4704-4719
The original publication is available at http://onlinelibrary.wiley.com doi:10.1002/hyp.10987

187 homogeneous soil case. For water flow, the experimental soil hydraulic properties (i.e., water
188 retention curve and saturated hydraulic conductivity) were considered as the initial parameters
189 set. For heat transport, the parameters of the apparent thermal conductivity, described using the
190 Laurent and Guerre-Chaley model (Laurent and Guerre-Chaley, 1995) were used. Then, to
191 improve model predictions, these parameters were calibrated as described later.

192 As initial conditions, we used linearly interpolated *h* and *T* profiles from the experimental
193 measurements at nine depths in the soil profile. For the water transport bottom boundary
194 condition, a known water flux equal to the evaporation flux at the surface was used. On the other
195 hand, constant average daily temperatures of 11.42 and 13.90°C, which were imposed for the
196 0.75 m and 0.40 m water table levels, respectively, were used as the bottom boundary condition
197 for heat transport. The choice of the water transfer bottom boundary condition is consistent with
198 the experimental conditions, where the soil column was replenished daily from the bottom to
199 compensate for surface evaporation. Another type of boundary condition, where a constant
200 pressure (i.e. the water table depth) is imposed at the bottom of the domain, was also tested and is
201 discussed in the sensitivity analysis discussed in section 4.2. Also, note that the temperatures at
202 the bottom for the 0.75 and 0.40 m water table levels are different because even when the
203 experiments were conducted successively, they were carried out at different times of the year.
204 The temperature values correspond to an extrapolation of the data measured at 50 cm depth. The
205 upper boundary condition was adapted to the laboratory experimental conditions since it was not
206 possible to compute the surface energy balance as required by SiSPAT. In the upper boundary,
207 surface temperature, relative humidity and wind speed measurements were used to calculate the
208 evaporation flux (Braud et al., 2009b). These measurements were included in the model as

Author-produced version of the article published in Hydrological Processes (2016), 30 25: 4704-4719
The original publication is available at http://onlinelibrary.wiley.com doi:10.1002/hyp.10987

follows: air temperature T_a (K) and relative humidity H_r (-) were measured at a reference level z_{at} = 0.01 m, and the wind speed U_a (m s^{-1}) at a reference level z_{av} = 0.3 m. Bare soil evaporation, E (m s^{-1}), was calculated using the following equation:

$$E = \rho_a \frac{(q_s - q_a)}{R_{aH}} \quad (5)$$

where ρ_a (kg m^{-3}) is the air density, R_{aH} (s m^{-1}) is the aerodynamic resistance to heat and water vapor transfer, and q_s (-) and q_a (-) are the soil and air surface specific humidity, respectively. q_s and q_a are related to the soil surface temperature T_s (K), the air temperature T_a (K), and the relative humidity of the soil H_{rs} (-) and the air H_a (-) by:

$$q_s = \frac{0.622\, e_{sat}(T_s)\, H_{rs}}{P_{atm} - 0.378\, e_{sat}(T_s)\, H_{rs}} \quad (6)$$

$$q_a = \frac{0.622\, e_{sat}(T_a)\, H_a}{P_{atm} - 0.378\, e_{sat}(T_a)\, H_a} \quad (7)$$

$$H_{rs} = \exp\left(\frac{Mgh}{RT_a}\right) \quad (8)$$

where P_{atm} (Pa) is the atmospheric pressure, R (J mol^{-1} K^{-1}) is the gas constant, M (kg mol^{-1}) is the molecular weight of water and $e_{sat}(T)$ is the saturated vapor pressure at a temperature T. The value of q_s at the soil surface (z = 0) was computed using the simulated values of soil temperature and soil water pressure in Eqs. (6) and (8).

The aerodynamic resistance to heat and water vapor transfer (R_{aH}) is defined as (Boulet et al., 2000):

Author-produced version of the article published in Hydrological Processes (2016), 30 25: 4704-4719
The original publication is available at http://onlinelibrary.wiley.com doi:10.1002/hyp.10987

$$R_{aH} = R_{ao}(1+Stab)^{-2} \qquad Stab \le 0$$
$$R_{aH} = R_{ao}(1+Stab)^{-0.75} \qquad Stab \ge 0 \tag{9}$$

where *Stab* (-) is a stability parameter and R_{ao} (s m^{-1}) is the aerodynamic resistance under neutral conditions. The stability parameter enables the atmosphere stratification to be taken into account, and is defined as (Boulet et al., 2000):

$$Stab = \frac{5\, g\, z_{at}\, (T_s - T_a)}{T_a\, U_a^2} \tag{10}$$

Finally, the aerodynamic resistance under neutral conditions is defined as (Shuttleworth and Wallace, 1985; Liu et al., 2007):

$$R_{ao} = \frac{1}{k^2 U_a}\left[\ln\left(\frac{z_{at}}{z_{om}}\right)\right]^2 \tag{11}$$

where z_{om} (m) is the roughness length for momentum, and $k \approx 0.4$ (-) is the von Karman constant.

2.3.3 Calibration procedure and calibration metrics

As described before, the experimental soil hydraulic properties were used as the initial parameters set to run the model. As the soil was packed homogeneously in the soil column, these properties were assumed to be uniform within the soil profile. Then, these properties were adjusted to fit the modeled results to the evaporation experiments observations. The model parameters were fitted manually, based on the comparison of modeled and observed soil volumetric water content and temperature profiles. Once the parameters were fitted, the cumulative evaporation simulated at the soil surface was compared to the experimental

Author-produced version of the article published in Hydrological Processes (2016), 30 25: 4704-4719
The original publication is available at http://onlinelibrary.wiley.com doi:10.1002/hyp.10987

cumulative evaporation. The calibration metrics used to quantify the goodness of fit were the root mean square error (*RMSE*), the bias (*B*), and the Nash-Sutcliffe efficiency (*E*):

$$RMSE = \sqrt{\frac{1}{n}\left(y_i^{\mathrm{mod}} - y_i^{obs}\right)^2} \tag{12}$$

$$B = \frac{1}{n}\sum_{i=1}^{i=n}\left(y_i^{\mathrm{mod}} - y_i^{obs}\right) \tag{13}$$

$$E = 1 - \frac{\sum_{i=1}^{i=n}\left(y_i^{\mathrm{mod}} - y_i^{obs}\right)^2}{\sum_{i=1}^{i=n}\left(\bar{y}^{obs} - y_i^{obs}\right)^2} \tag{14}$$

where y_i^{mod} are the modeled values, y_i^{obs} the corresponding observed values, and y^{obs} is the average value of all observed data. These statistics were computed using the observed profiles of temperature and soil water content at the end of the experiment and the modelled values at the same depths.

2.4 Sensitivity analysis

A sensitivity analysis can provide valuable information about the evaporation mechanisms and the role of various parameters on these mechanisms. In our sensitivity analysis, the impact of the variation of different parameters on cumulative evaporation was assessed. Although the processes involved in evaporation are strongly coupled, we focused the sensitivity analysis on two parameters of the vapor flow component: tortuosity (τ_a) and the enhancement factor (η), which are the most uncertain parameters in the isothermal and thermal water vapour fluxes respectively.

Author-produced version of the article published in Hydrological Processes (2016), 30 25: 4704-4719
The original publication is available at http://onlinelibrary.wiley.com doi:10.1002/hyp.10987

In the literature, there are several expressions to determine the tortuosity, which has values less than 1.0 (Penman, 1940; Millington and Quirk, 1961; Abu-El-Sha'r and Abriola, 1997). In the sensitivity analysis, we considered several constant tortuosity values in the soil profile, ranging between 0.1 and 0.3; and the expression of the tortuosity factor proposed by Millington and Quirk (1961), as reported by Saito et al. (2006):

$$\tau_a = \frac{a_v^{7/3}}{\theta_s^2} = \frac{(\theta_s - \theta)^{7/3}}{\theta_s^2} \quad (15)$$

where a_v (m^3 m^{-3}) is the air content.

The sensitivity analysis related to the enhancement factor value consisted in evaluating constant values ranging between 1.5 and 3.0, as reported by Philip and de Vries (1957). We also evaluated the enhancement factor using the expression reported by Cass et al. (1984):

$$\eta = a + 3\frac{\theta}{\theta_S} - (a-1)\exp\left\{-\left[\left(1+\frac{2.6}{\sqrt{f_C}}\right)\frac{\theta}{\theta_S}\right]^3\right\} \quad (16)$$

where f_c is the clay fraction of the soil studied and a is an adjustment factor that was varied between 3.0 and 9.5. Note that the reference simulation discussed in section 3.2 was performed using η = 1.5 and the tortuosity given by Eq. (15).

3 Results

3.1 Summary of experimental results, simulations with vertically uniform hydraulic properties, and calibration of model parameters

Author-produced version of the article published in Hydrological Processes (2016), 30 25: 4704-4719
The original publication is available at http://onlinelibrary.wiley.com doi:10.1002/hyp.10987

Figure 1 shows the experimental and modeled soil water content (θ) and thermal (T) profiles, for the 0.75 and 0.40 m water table levels. The modeled results were obtained assuming a soil profile that has vertically uniform hydraulic properties. Figure 1 also shows the corresponding observed electrical conductivity (σ) profiles. The experimental and modeled results depicted in Figure 1 correspond to the mean daily values after ~20 days of fixing the water table level. The soil column experiments began with a dry soil and then the water table was fixed at a depth of 0.75 m. After ~20 days, the electrical conductivity profile showed a zone of increased conductivity (~0.2-0.3 m depth) that is correlated to a zone of increased moisture content.

The simulation results presented in Figure 1 highlights the inability of the numerical model to correctly represent the hydraulic and thermal behavior assuming a vertically homogeneous soil and using the soil hydraulic properties obtained from independent laboratory experiments. From Figure 1 it is clear that using spatially uniform soil's hydrodynamic properties in the modeling exercise does not allow a correct simulation of the experimental soil moisture and thermal profiles for both water table levels. Additional sensitivity analyses showed that it is not possible to reproduce the observed profiles when the hydrodynamic properties are considered uniform along the soil profile (data not shown).

Figure 2 shows the mean observed and modeled soil water content and temperature profiles on day 20 for the 0.75 and 0.40 m water table levels, when using the optimized parameters for each horizon in the soil profile. For the 0.75 m water table level, the thicknesses of the soil horizons were: 0.20 m for horizon 1 (H1); 0.10 m for horizon 2 (H2); and 0.90 m for

Author-produced version of the article published in Hydrological Processes (2016), 30 25: 4704-4719
The original publication is available at http://onlinelibrary.wiley.com doi:10.1002/hyp.10987

298 horizon 3 (H3). For the 0.40 m water table level, the thicknesses of the soil horizons were: 0.15 m
299 for H1; 0.15 m for H2; and 0.90 m for H3. These thicknesses were determined according to the
300 experimental results presented by Hernández-López et al. (2014). Table 3 presents the values of
301 the parameters obtained in the calibration process. After calibrating the soil hydraulic and thermal
302 properties, the model results agree fairly well with the experimental data and suggest that the
303 only way to represent water and heat transport in these experiments is by accounting for the soil
304 properties spatial variability, which are likely to be modified as a consequence of salt transport
305 and precipitation/dissolution reactions (Vásquez et al., 2013; Fierro, 2015; Nachshon and
306 Weisbrod, 2015).

307 Table 4 presents the calibration metrics obtained after considering the three soil horizons
308 and the experimental and modeled cumulative evaporation values, for both the 0.75 and of 0.40
309 m water table levels. The values of the *RMSE*, *B*, and *E* for soil water content and temperature are
310 very good for the 0.75 m water table depth and lower for the 0.4 m water table depth. The
311 calibrated model correctly reproduces the observed evaporation values from the laboratory
312 measurements, with differences of ~0.01 mm in the cumulative evaporation for the 0.75 m water
313 table depth and ~0.67 mm for the 0.40 m water table depth. Also, by simultaneously reproducing
314 the soil water content and the thermal profiles, and the cumulative evaporation, the problem of
315 equifinality is minimized (Tang and Zhuang, 2008) (this is discussed in more details in the
316 sensitivity analysis). These results highlight the importance of calibrating the model parameters
317 for each water table level in order to obtain a better estimate of the main mechanism that govern
318 the evaporation fluxes.

Author-produced version of the article published in Hydrological Processes (2016), 30 25: 4704-4719
The original publication is available at http://onlinelibrary.wiley.com doi:10.1002/hyp.10987

3.2 Simulation of liquid water and water vapor fluxes to locate the evaporation front and sensitivity analysis

The evaporation fluxes are related to vapor transfer due to temperature and pressure gradients (Boulet et al., 1997). Figures 3 (a) and (b) show the total water flux, q_T, the liquid water flux, q_L, and water vapor flux, q_v, profiles for the 0.75 and 0.40 m water table depths, respectively. Figures 3 (c) and (d) present the vapor fluxes due to thermal (q_{vT}) and pressure (q_{vh}) gradients for the 0.75 and 0.40 m water table levels. From these results, three regions can be distinguished in the soil profile: (1) *Region 1*, located near to the soil surface, between 0 and 0.12 m for the 0.75 m water table level and between 0 and 0.03 m for the 0.40 m water table level; (2) *Region 2*, located between 0.12 and 0.41 m for the 0.75 m water table level and between 0.03 and 0.32 m for the 0.40 m water table level; and (3) *Region 3*, located between 0.41 and 0.75 m for the 0.75 m water table level, and between 0.32 and 0.40 m for the 0.40 m water table level.

Our sensitivity analysis focused on determining how the tortuosity (τ_a) and the enhancement factor (η) affect the cumulative evaporation. These parameters were selected for the sensitivity analysis because τ_a is the most uncertain parameter used to determine the isothermal diffusivity (D_{vh}), and η is the parameter with greater uncertainty when calculating the thermal diffusivity (D_{vT}). Figure 4 presents the results of the sensitivity analysis. On one hand, when τ_a increases, the cumulative evaporation also increases. On the other hand, when η increases (i.e., when the *a* parameter of the Cass et al. (1984) model increases), the cumulative evaporation decreases.

Author-produced version of the article published in Hydrological Processes (2016), 30 25: 4704-4719
The original publication is available at http://onlinelibrary.wiley.com doi:10.1002/hyp.10987

4 Discussion

4.1 Experimental results, simulations with vertically uniform hydraulic properties, and calibration of model parameters

The results of the experiments are discussed in details in Hernandez-Lopez et al. (2014) and here we only present the main findings that are relevant for this modelling study. Because the column was homogeneously packed before the evaporation experiments, the zone of increased electrical conductivity and moisture shown in Figure 1 is likely to be the result of salt movement towards the soil surface as evaporation occurred (Nachshon et al., 2011), and also due to salt transport as the water level rose. We believe that these salt-transport processes resulted in soil stratification (in terms of salt deposition) and soil hydraulic properties that are no more vertically homogeneous. Note also that there was no evidence of spatial heterogeneity across the soil surface or preferential flow along the sidewalls of the soil column. For the 0.4 m deep water table level, electrical conductivity and soil water content profiles increased at all horizons, as compared to the profiles obtained when the water table was at 0.75 m depth. This increased water content profile is a consequence of the increased liquid water transport by capillarity. Such a movement was favored in our experimental conditions because we wetted the soil from below as the water table rose. In the zone between ~0.2-0.3 m depth, this increased water content may also be due to salt accumulation (Scotter, 1974). According to the electrical conductivity profiles, salt crystallized in the smallest pores in the soil as subflorescent precipitation. This crystallization decreases the pore space in the soil matrix and therefore decreases the K_s (Nachshon et al., 2011; Vásquez et al., 2013), reduces the vapor flow (Nachshon and Weisbrod, 2015), and also modifies the water retention characteristics (as described below) (Fierro, 2015). Although subflorescent

precipitation has been widely investigated in other disciplines, few investigations have reported this type of precipitation in soils under drying conditions (Weisbrod et al., 2013; Sghaier et al., 2014). To our best knowledge, the present work is the first one reporting probable subflorescence precipitation in laboratory columns designed to study water movement in soils where the water table is rising. Although subflorescence was not directly measured, we rely on electrical conductivity measurements to evidence this phenomenon. More detailed measurements would have been required to clearly show the subflorescence. Moreover, most of the studies that investigate salt precipitation in soils have been performed with initially saturated soil columns where efflorescent precipitation or formation of a salt crust was observed at the surface of the column when the water table was lowered (Gran et al., 2011; Nachshon et al., 2011).

The soil water content and electrical conductivity profiles shown in Figure 1 evidenced salt transport and a probable salt accumulation within the soil column (Hernández-López et al., 2014). Unfortunately, we did not quantify the deposited salts within the pores using visual techniques such as microscopic imaging. Nonetheless, the electrical conductivity, as an indirect measure of salinity, showed the existence of three horizons resulting from the transport and accumulation of salt in the soil column. Therefore, it is very likely that transport, dissolution and precipitation of salts modified the hydrodynamic properties of the soil as evaporation occurred (Benavente et al., 1999; Fierro, 2015; Nachshon and Weisbrod, 2015). All this literature review shows that there is still no clear consensus about the impact of salt precipitation inside salty soils and more experimental studies, with enhanced capabilities to observe salt movement and precipitation would be required.

Author-produced version of the article published in Hydrological Processes (2016), 30 25: 4704-4719
The original publication is available at http://onlinelibrary.wiley.com doi:10.1002/hyp.10987

382 To address the spatial variability of the soil properties, we divided the soil profile intro
383 three horizons of different thicknesses for the two studied water table levels. For each horizon we
384 optimized their hydrodynamic and thermal properties to fit the observed values, which produced
385 the parameters presented in Table 3. This approach overcomes the limitation of the SiSPAT
386 model, which does not account for salt transport, but increases significantly the number of
387 parameters. As the objective was to analyze the calculated evaporation fluxes, we consider that
388 the model should simulate the moisture and thermal profiles as close as possible to those
389 observed, in order to accomplish the correct interpretation.

390 Figure 5 compares the experimental water retention curve and those fitted for the three
391 horizons of the soil profile (for water tables located at 0.75 and 0.40 m depth). For both water
392 table depths, the shallower soil horizons (H1 and H2) show an increase in their capacity to retain
393 water, while the deeper horizon (H3) shows the opposite trend and reduces its capacity to hold
394 water. Even when the fitted water retention curves show small differences when compared to the
395 vertically uniform water retention properties, the changes are relevant to describe the water
396 content and temperature profile within the soil column. The fitted water retention curves (Figure
397 5) for horizons H1, H2 and H3 show a behavior that is consistent with upward salt transport. The
398 salts that were in the lower parts of the soil matrix dissolved as the soil column wetted from
399 below. This dissolution increased the pore size and reduced the capacity of the soil to retain
400 water. As the salts were dissolved in the lower parts of the soil column, they began to move
401 upwards as a consequence of the evaporation fluxes. Once the liquid water evaporated at
402 shallower parts of the soil, salts are being accumulated and precipitation reactions occur. This salt
403 precipitation increases the capacity of the soil to retain water, which can occur due to a reduction

in the pore space (Vásquez et al., 2013) or due to hygroscopy (Tóth et al., 2012), which is the ability of the salts to attract and retain water molecules from the surroundings. Even when the fitted water retention curves show minor differences when compared to the vertically uniform water retention curve derived from experimental measurements, their changes are relevant for describing the moisture and thermal dynamics within the soil (Figures 1 and 2). These results are in agreement with those obtained by Fierro (2015). The most significant variation in the hydraulic parameters are associated with those related to the hydraulic conductivity curve (K_s and β) for the 0.40 m water table level. The K_s values fitted for this water table are very small for the two shallower horizons (i.e., H1 and H2) and do not correspond to the type of soil used. This hydraulic conductivity reduction is likely due to a higher concentration of salts that could lead to precipitation reactions, which then reduce the water flow paths (Vásquez et al., 2013). Note also that in the experiments of Nachshon and Weisbrod (2015) subflorescent salt precipitation reduced the pore space. As a consequence, there is a potential decrease in the unsaturated hydraulic conductivity (Wissmeier and Barry, 2008). However, this pore space reduction in the liquid flow path did not limit the evaporation rates in the experiments of Nachshon and Weisbrod (2015). Therefore, in their experiments, which began with saturated conditions in the soil profile, the evaporation rates were controlled by the diffusive vapor transport between the matrix surface and the atmosphere.

4.2 Simulation of liquid water and water vapor fluxes to locate the evaporation front and sensitivity analysis

Author-produced version of the article published in Hydrological Processes (2016), 30 25: 4704-4719
The original publication is available at http://onlinelibrary.wiley.com doi:10.1002/hyp.10987

As described before, from the simulation results three regions can be distinguished in the soil profile (Figure 3). In *region 1*, the total flux is directed upwards and the water movement is mainly due to vapor fluxes driven by pressure gradients. Although in this area isothermal upwards vapor fluxes and thermal downwards vapor fluxes coexist, the isothermal vapor flux (q_{vh}) is larger than the thermal vapor flux (q_{vT}). In this area, the evaporation front is located where the liquid and water vapor fluxes are equal (Braud et al., 2005a; 2009b; Hernández-López et al., 2014), i.e., at depths of 0.12 and 0.03 m for 0.75 and 0.40 m water table levels, respectively. In *region 2* for the 0.75 m water table depth, the liquid water flux dominates and net water transfer is directed upwards. On the contrary, when the water table was located at 0.40 m depth, the net water transfer is directed downwards (being the liquid water flux the main water transfer mechanism). This downward liquid flux implies a condensation process within the soil profile, which may contribute to water storage in this portion of the soil (unfortunately, such condensation was not measured experimentally due to the low vertical resolution of the observations). In this area, the isothermal vapor flux is zero and the downwards thermal vapor flow is smaller as depth increases. In *region 3*, the water vapor flux is very small. These results indicate that evaporation occurs in the upper soil profile, and that the position of the evaporation front is closer to the soil surface as the water table depth reduces. In the area close to the surface where evaporation takes place, the upward vapor flux caused by pressure gradients is larger than the downward vapor flux due to temperature gradients (Konukcu et al., 2004; Gran et al., 2011; Hernández-López et al., 2014).

It is interesting to note that the experiments of Hernández et al. (2014) assumed that steady state was reached when the experimental variables varied in less than 1%. However, in the

Author-produced version of the article published in Hydrological Processes (2016), 30 25: 4704-4719
The original publication is available at http://onlinelibrary.wiley.com doi:10.1002/hyp.10987

previous discussion the directions of the net water flux in *regions 1* and *2* are different, which contradicts the principle of mass conservation under steady state conditions. Because the SiSPAT model has been conceived to respect the energy and mass balance, and it has proven its robustness for isotopic transport in very constraining conditions (see for instance Braud et al., 2005a), mass conservation is being correctly solved in the model. Therefore, even when the experimental variables did not changed significantly after 20 days of fixing the water level, the system is likely to be under transient conditions. Note also that the experimental conditions of Hernández-López et al. (2014), may not favor steady state establishment because although the laboratory temperature and humidity were controlled; the forcing temperature above the soil column and at the bottom of the column was varying in time. When analyzing the model results, there is a change in soil moisture storage, even after 20 days, and the sign of change in water content is consistent with the explanation provided in the previous paragraph in terms of fluxes directions. In this case, even if the fluxes at the top and at the bottom of the soil column were the same, steady state was not reached after 20 days as the total flux inside the intermediate part of the column was not equal to that modeled at the boundaries. We tested a run lasting 500 days to see if it was possible to reach steady state and we found that for the 0.75-m water table depth, steady state was reached after ~150 days with soil water content and temperature profiles very similar to those shown in Figure 2 (see Figure 6). For the 0.40-m water table depth, the time to reach steady state was longer (~400 days) and the shape of the profile is quite different, as shown in Figure 6. These results suggest that the experiments performed by Hernández-López et al. (2014) were not under steady state conditions after 20 days of fixing the water table level.

Author-produced version of the article published in Hydrological Processes (2016), 30 25: 4704-4719
The original publication is available at http://onlinelibrary.wiley.com doi:10.1002/hyp.10987

Additional simulations were also performed to test the impact of the choice of the bottom boundary condition on the results. In these simulations, the known flux equal to the evaporation rate at the top of the soil profile was replaced with a known pressure of 0.45 m (to simulate a water table depth at 0.75 m from the surface of the 1.2-m depth column). With this boundary condition (imposed soil water pressure), it was found that after 500 days steady state conditions were not achieved and the simulation results were not realistic. In fact, given the model configuration, drainage was simulated at the bottom of the column.

The analysis of these results shows the value of running a physical model in parallel to laboratory experiments as the model provides information and explanation about possible active processes that are not accessible to the experimental observations. Especially in terms of the interplay between liquid and vapor fluxes. The physical model also allows testing various boundary conditions and soil hydraulic properties, which would not be accessible using laboratory experiments only.

It is important to point out that from the experimental results, as discussed by Hernández-López et al. (2014), it is not easy to locate the evaporation front. This issue occurred because of the too low spatial resolution (0.05 m) of the instruments used in their experiments. From the thermal profile when the water table was at 0.75 m depth, Hernández-López et al. (2014) estimated that the location of the evaporation front was between the soil surface and a depth of ~0.10 m. For shallower water tables, Hernández-López et al. (2014) were unable to determine the position of the evaporation front and only concluded that it was located between the soil surface and ~0.05 m depth (the location of their shallowest sensor). This difficulty can be overcome with

Author-produced version of the article published in Hydrological Processes (2016), 30 25: 4704-4719
The original publication is available at http://onlinelibrary.wiley.com doi:10.1002/hyp.10987

high resolution measurements or with the use of a numerical model. Indeed, our numerical model allowed determining the evaporation front (0.12 and 0.03 m when the water table was at 0.75 and 0.40 m depth, respectively). Note also that, as described before, the location of the evaporation front obtained from the numerical model agrees fairly well with the observations of Hernández-López et al. (2014).

The sensitivity analysis permitted to understand how the enhancement and tortuosity factors affect cumulative evaporation (Figure 4). In terms of the enhancement factor, Cass et al. (1984) recommend using a = 9.5 for a sandy textured soil when determining η using equation (16). Although the Cass et al. (1984) model is generally accepted to determine the vapor thermal diffusivity, the recommended value of a does not lead to an acceptable fit with the experimental values. On the contrary, Philip and de Vries (1957) suggests η = 1.5 for sandy soils. This value of η yields simulated cumulative evaporation values more consistent with those observed in the experiments (Hernández-López et al., 2014). Note also that when τ_a is calculated using the expression proposed by Millington and Quirk (1961), the cumulative evaporation for both experiments are simulated correctly.

Figure 7 compares the vapor fluxes (q_v) for the different values of τ_a and η presented in Figure 4, and for both water table levels. In general, when τ_a increases, the vapor flux increases in the upward direction. This behavior is more evident between ~0-0.13 m depth when the water table level was at 0.75 m, and between ~0-0.05 m depth when the water table was at 0.40 m. It is also interesting to observe that for large values of η, the net water flux direction changes from upwards to downwards. Moreover, when η increases, condensation at the soil surface occurs

Author-produced version of the article published in Hydrological Processes (2016), 30 25: 4704-4719
The original publication is available at http://onlinelibrary.wiley.com doi:10.1002/hyp.10987

(Figures 4 and 6). In addition to the magnitude and direction, in some cases the position of the evaporation front also changes. By increasing τ_a, the evaporation front is located deeper in the soil (starting from the surface of the soil).

Although changes in cumulative evaporation and vapor flux due to changes in τ_a are important, the influence of variations in η is even more significant, resulting sometimes in major condensation. These results, which disagree with the experimental observations, allow discarding different set of calibrated parameters that yields non-physical results and thus, minimize the problem of equifinality. For instance, as shown in Figure 4 for a water table located at 0.75 m depth and using a variable η (equation (16) with $a \geq 4.0$), even when the soil water content and the temperature profiles are represented satisfactorily, the modeled cumulative evaporation after reaching quasi steady state is negative, i.e., the model predicts water condensation at the soil surface. Instead, the experimental observations show a cumulative evaporation of ~0.9 mm.

4.3 Model limitations

Our approach has some limitations that need to be understood in order to perform a correct interpretation of the results. One important aspect that the SiSPAT model does not represent is fluid flow due to solute concentration effects (Barbour and Fredlund, 1989; Nachshon et al., 2011). Indeed, as shown by Nassar et al. (1989), the osmotic gradient can be an important driving force for water movement in unsaturated soils with high clay content. We used the approach proposed by Barbour and Fredlund (1989) to determine the order of magnitude of the liquid and water vapor fluxes due to solute concentration gradients. In this analysis, we assumed that sodium chloride (NaCl) was the main component that contributes to the osmotic

Author-produced version of the article published in Hydrological Processes (2016), 30 25: 4704-4719
The original publication is available at http://onlinelibrary.wiley.com doi:10.1002/hyp.10987

pressure and that the maximum solute concentration occurred at saturated conditions (~25 wt% for NaCl). Also, the observed experimental conditions were utilized to evaluate the temperature in the Van't Hoff equation (Barbour and Fredlund, 1989), and the experimental soil water content was used to determine the osmotic flow of water within the soil. This analysis resulted in osmotic fluid flows on the order of 10^{-11} m/s, which are at least one order of magnitude smaller than those obtained using SiSPAT. Thus, in our experiments we expect a small contribution of the osmotic flow of water in the liquid and the gaseous phase.

It is also important to discuss that discrepancy between experimental data and model predictions has led to the development of vapor-flux enhancement factors, such as η (Philip and de Vries, 1957; Cass et al., 1984). The inclusion of these enhancement factors in numerical models, such as that used in this work, is due to a lack of sufficiently accurate description of vapor dynamics to represent correctly the soil physics processes that occur during evaporation (Assouline et al., 2013). There are many processes that explain this vapor-flux enhancement (Philip and de Vries, 1957; Cass et al., 1984; Bachmann et al., 2001; Grifoll et al., 2005; Shokri et al., 2009; Shahraeeni and Or, 2012; Assouline et al., 2013; Trautz et al., 2015). For instance, investigations have shown that with proper account of capillary flow, continuity and pathways, no vapor-flux enhancement factors are required (Grifoll et al., 2005; Shokri et al., 2009). Shahraeeni and Or (2012) demonstrated that water transport can be enhanced by ~10% when isolated liquid-phase bridges are present due to a reduction in the gaseous diffusion path length, and that thermal gradients can enhance water vapor diffusion. Also, vapor flux from within the soil profile can be enhanced by thermally driven convective transport mechanisms (Bachmann et

Author-produced version of the article published in Hydrological Processes (2016), 30 25: 4704-4719
The original publication is available at http://onlinelibrary.wiley.com doi:10.1002/hyp.10987

551 al., 2001). Recently, Trautz et al. (2015) argued that non-equilibrium phase change is also
552 responsible for vapor-flux enhancement.

553 From the vapor-flux enhancement mechanisms that have been reported in the scientific
554 literature, we hypothesize that a combination between non-equilibrium phase change and cyclic
555 thermal conditions typically found between day and night, could be responsible for the vapor-flux
556 enhancement observed in our experiments. When cyclic thermal conditions are present, two
557 processes can drive soil evaporation: evaporation from the soil surface into the atmosphere during
558 early morning and subsurface evaporation limited by Fickian Diffusion until late afternoon. As
559 explained by Assouline et al. (2013), evaporation from the soil surface depletes the water
560 condensed and redistributed during nighttime. After the depletion of this water, Fickian diffusion
561 becomes the governing process and increases the thickness of the dry layer of soil observed at the
562 soil surface. In addition, as discussed by Trautz et al. (2015), non-equilibrium processes are
563 relevant when cyclic thermal conditions occur.

564 Many studies have used laboratory columns, but very few of them have focused on
565 understanding natural highly saline dry soils. Moreover, typical column experiments do not deal
566 with natural highly salty soils and low water content. Our results show that evaporation in
567 initially dry soils produce moisture content and conductivity distributions that are atypical. This
568 behavior has not been reported in the literature, which typically reports experiments in which an
569 initially saturated soil column is subsequently dried out.

570 ## 5. Conclusions

Author-produced version of the article published in Hydrological Processes (2016), 30 25: 4704-4719
The original publication is available at http://onlinelibrary.wiley.com doi:10.1002/hyp.10987

571 To improve the understanding of bare soil evaporation, which is typically the main source
572 of aquifer depletion in zones such as those located in the Altiplano basins of northern Chile, we
573 conducted a modeling study to investigate evaporation processes under non-isothermal
574 conditions. A model that couples liquid water, water vapor, and heat transport was developed and
575 calibrated using laboratory observations performed in a homogeneous natural soil column that
576 was filled with soil from the Huasco salt flat, Chile. Modeled and experimental results only
577 agreed when the soil hydrodynamic properties (water retention and hydraulic conductivity curve)
578 were calibrated. The change in the soil hydrodynamic properties can be explained by
579 precipitation/dissolution reactions that are driven by evaporation and that yield a stratified soil
580 profile when quasi steady state conditions were achieved.

581 Model results showed a good agreement with the experimental observations of the soil
582 water content and thermal profiles, and also reproduced the experimental cumulative evaporation
583 with differences of 0.01 and 0.67 mm for the 0.75 and 0.40 m water table depths, respectively.
584 Model results permitted to distinguish three characteristic zones in the soil profile. The first zone
585 (*region 1*) is located near the surface, where the total flux is directed upwards and the water
586 movement is mainly due to vapor fluxes driven by pressure gradients. The second zone (*region 2*)
587 is located below *region 1* and is where the liquid water flux dominates. The third zone (*region 3*)
588 is where the liquid water flux is very small. Model results indicate that evaporation occurs in the
589 upper soil profile and that the position of the evaporation front depends on the water table depth.

590 A sensitivity analysis allowed understanding the impact of the enhancement factor and the
591 tortuosity on the cumulative evaporation. The enhancement factor had the largest influence on

cumulative evaporation that can even result in condensation at the soil surface. This analysis also allowed discarding different set of calibrated parameters that yield non-physical conditions, which minimize the problem of equifinality. The results presented in this study are important as they allow understanding the main evaporation processes that occur in bare soils from Altiplano basins where these processes are not well understood.

Acknowledgments

The authors acknowledge funding from the Chilean National Commission for Scientific and Technological Research (CONICYT/FONDECYT/1130522). F. Suárez and J. Gironás thank the Centro de Desarrollo Urbano Sustentable for additional support (CEDEUS - CONICYT/FONDAP/15110020), and J. Gironás also acknowledges the Centro de Investigación para la Gestión Integrada de Desastres Naturales (CIGIDEN - CONICYT/FONDAP/15110017). The modeling study presented in this paper was possible thanks to a grant for a stay of M.F. Hernández-López at Irstea, funded by Pontificia Universidad Católica de Chile and Irstea. We also thank the anonymous reviewers for the positive comments that improved this paper.

References

Abu-El-Sha'r WY, Abriola LM. 1997. Experimental assessment of gas transport mechanisms in natural porous media: parameter evaluation. Water Resource Research, 33(4): 505-516.

Alazard M, Leduc C, Travi Y, Boulet G, Ben Salem A. 2015. Estimating evaporation in semi-arid areas facing data scarcity: example of the El Haouareb dam (Merguellil catchment, Central Tunisia). Journal of Hydrology: Regional Studies 3:265-284.

612 Assouline S, Tyler SW, Selker JS, Lunati I, Higgins CW, Parlange MB. 2013. Evaporation from
613 a shallow water table: diurnal dynamics of water and heat at the surface of drying sand.
614 Water Resources Research, 49:4022-4034.
615 Bachmann J, Horton R, van del Ploeg RR. 2001. Isothermal and nonisothermal evaporation from
616 four Sandy soils of different water repelency. Soil Sci. Soc. Am. J., 65, 1599-1607.
617 Barbour SL, Fredlund DG. 1989. Mechanisms of osmotic flow and volume change in clay soils.
618 Can. Geotech. J., 26, 551-562.
619 Benavente D, García del Cura MA, Fort R, Ordónez S. 1999. Thermodynamic modelling of
620 changes induced by salt pressure crystallisation in porous media of stone. Journal of Crystal
621 Growth, 204: 168-178.
622 Boulet G, Braud I, Vauclin M. 1997. Study of the mechanisms of evaporation under arid
623 conditions using a detailed model of the soil-atmosphere continuum. Application to the
624 EFEDA I experiment. Journal of Hydrology, 193(1-4): 114-141.
625 Boulet G, Chehbouni A, Braud I, Vauclin M, Haverkamp R, Zammit C. 2000. A simple water
626 and energy balance model designed for regionalization and remote sensing data utilization.
627 Agricultural and Forest Meteorology, 105: 117-132.
628 Braud I, Bariac T, Gaudet JP, Vauclin M. 2005a. SiSPAT-Isotope, a coupled heat, water and
629 stable isotope (HDO and H218O) transport model for bare soil. Part I: Model description
630 and first verification, J. Hydrology, 309(1-4), 277-300.
631 Braud I, Bariac T, Vauclin M, Boujamlaoui Z, Gaudet JP, Biron Ph, Richard P. 2005b. SiSPAT-
632 Isotope, a coupled heat, water and stable isotope (HDO and H218O) transport model for

633 bare soil. Part II: Evaluation and sensitivity tests using two laboratory data sets, J.
634 Hydrology, 309(1-4), 301-320.
635 Braud I, Biron P, Bariac T, Richard P, Canale L, Gaudet JP, Vauclin M. 2009a. Isotopic
636 composition of bare soil evaporated water vapor. Part I: RUBIC IV experimental setup and
637 results. Journal of Hydrology, 369: 1-16.
638 Braud I, Bariac T, Biron P, Vauclin M. 2009b. Isotopic composition of bare soil evaporated water
639 flow. Part II: Modeling of RUBIC IV experimental results. Journal of Hydrology, 369: 17-
640 29.
641 Braud I, Dantas-Antonino AC, Vauclin M, Thony JL, Ruelle P. 1995. A simple soil-plant-
642 atmosphere transfer model (SiSPAT) development and field verification. Journal of
643 Hydrology, 166: 213-250.
644 Brooks RH, Corey AT, 1964. Hydraulic properties of porous media. Hydrology paper 3,
645 Colorado State University, Fort Collins, 27 pp.
646 Cahill AT, Parlange MB, 1998. On water vapor transport in field soils. Water Resources
647 Research, 34(4): 731-739.
648 Cass A, Campbell GS, Jones TL. 1984. Enhacement of thermal water vapor difussion in soil. Soil
649 Science Society of America Proceedings, 48: 25-32.
650 de la Fuente A, Niño Y. 2010. Temporal and spatial features of the thermohydrodynamics of
651 shallow salty lagoons in northern Chile. Limnology and Oceanography 55:279-288.
652 Fierro V. 2015. SAR effects on evaporation fluxes from shallow groundwater. M. Sc. Thesis,
653 Pontificia Universidad Católica de Chile, Santiago, Chile.

654 Gran M, Carrera J, Massana J, Saaltink MW, Olivella S, Ayora C, Lloret A. 2011. Dynamics of
655 water vapor flux and water separation processes during evaporation from a salty dry soil.
656 Journal of Hydrology, 396: 215-220.
657 Grifoll J, Gastó JM, Cohen Y. 2005. Non-isothermal soil water transport and evaporation.
658 Advances in Water Resources, 28: 1254-1266.
659 Hernández-López MF, Gironás J, Braud I, Suárez F, Muñoz JF. 2014. Assessment of evaporation
660 and water fluxes in a column of dry saline soil subject to different water table levels.
661 Hydrological Processes, 28(10): 3655-3669.
662 Johnson E, Yáñez J, Ortiz C, Muñoz J. 2010. Evaporation from shallow groundwater in closed
663 basins in the Chilean Altiplano. Hidrological Sciences Journal, 55(4): 624-635.
664 Kampf S, Tyler S, Ortiz C, Muñoz J, Adkins P. 2005. Evaporation and land surface energy
665 budget at the Salar de Atacama, northern Chile. Journal of Hydrology 310:236–252.
666 Konukcu F, Istanbulluoglu A, Kocaman I. 2004. Determination of water content in drying soils:
667 incorporating transition from liquid phase to vapour phase. Australian Journal of Soil
668 Research 42(1): 1-8.
669 Laurent JP, Guerre-Chaley C. 1995. Influence de la teneur en eau et de la température sur la
670 conductivité thermique du béton cellulaire autoclave. Materials and Structures, 28:464-472.
671 Lictevout E, Maass C, Córdoba D, Herrera V, Payano R. 2013. Recursos Hídricos Región de
672 Tarapacá – Diagnóstico y Sistematización de la Información. CIDERH. ISBN:978 956 302
673 081 – 6. Available at: http://www.ciderh.cl/documentos/recursos-hidricos-region-de-
674 tarapaca/ (last accessed July 2016).

675 Liu S, Lu L, Mao D, Jia L. 2007. Evaluating parametrizations of aerodynamic resistance to heat
676 transfer using field measurements. Hydrology and Earth System Sciences, 11: 769-783.
677 Millington RJ, Quirk JM. 1961. Permeability of porous solids. 57. Transaction of the Faraday
678 Society, 57: 1200-1207.
679 Milly PCD. 1984. A simulation analysis of thermal effects on evaporation from soil. Water
680 Resources Research, 20(8): 1087-1098.
681 Nachshon U, Weisbroad N, Dragila MI, Grader A. 2011. Combined evaporation and salt
682 precipitation in homogeneous and heteregenous porous media. Water Resource Research,
683 47: W03513, doi:10.1029/2010WR009677.
684 Nachshon U, Weisbrod N. 2015. Beyond the Salt Crust: On Combined Evaporation and
685 Subflorescent Salt Precipitation in Porous Media. Transport in Porous Media, 110: 295-
686 310. DOI: 10.1007/s11242-015-0514-9.
687 Nassar IN, Horton R. 1989. Water transport in unsaturated nonisothermal salty soil: II.
688 Theoretical development. Soil Science Society of America Proceedings, 53: 1330-1337.
689 Novak MD. 2010. Dynamics of the near-surface evaporation zone and corresponding effects on
690 the surface energy balance of a drying bare soil. Agricultural and Forest Meteorology,
691 1501358-1365.
692 Penman HL. 1940. Gas and vapor movement in the soil. I. The diffusion of vapors through
693 porous solids. The Journal of Agricultural Science, 30(4): 570-581.
694 Philip JR, de Vries DA. 1957. Moisture movement in porous materials under temperature
695 gradient. Transactions American Geophysical Union, 38: 222-232.

696 Saito H, Simunek J, Mohanty BP. 2006. Numerical Analysis of Coupled Water, Vapor, and Heat
697 Transport in the Vadose Zone. Vadose Zone Journal, 5: 784-800.
698 Schulz S, Horovitz M, Rausch R, Michelsen N, Mallast U, Köhne M, Siebert C, Shüth C, Al-
699 Saud M, Merz R. 2015. Groundwater evaporation from salt pans: examples from the
700 eastern Arabian Peninsula. Journal of Hydrology. doi:10.1016/j.jhydrol.2015.10.048
701 Scotter DR. 1974. Salt and water movement in relatively dry soil. Australian Journal of Soil
702 Research, 12(1): 27-35.
703 Sghaier N, Geoffroy S, Prat M, Eloukabi H, Nasrallah SB. 2014. Evaporation-driven growth of
704 large crystallized salt structures in a porous medium. Phys. Rev. E 90, 042402
705 Shahraeeni E, Or D. 2012. Pore scale mechanisms for enhanced vapor transport through partially
706 saturated porous media. Water Resour. Res., 48, W05511, doi:10.1029/2011WR011036.
707 Shokri NP, Lehmann P, Or D. 2009. Critical evaluation of enhancement factors for vapor
708 transport through unsaturated porous media. Water Resour. Res., 45, W10433,
709 doi:10.1029/2009WR007769.
710 Shuttleworth WJ, Wallace JS. 1985. Evaporation from sparse crops an energy combination
711 theory. Quarterly Journal of the Royal Meteorological Society, 111: 839-855.
712 Tang J, Zhuang Q. 2008. Equifinality in parameterization of process-based biogeochemistry
713 models: A significant uncertainty source to the estimation of regional carbon dynamics,
714 Journal of Geophysical Research, 113, G04010, doi:10.1029/2008JG000757.
715 Tóth B, Makó A, Guadagnini A, Tóth G. 2012. Water retention of salt-affected soils: quantitative
716 estimation using soil survey information. Arid Land Research and Management 26:103-
717 121.

718 Trautz AC, Smits KM, Cihan A. 2015. Continuum-scale investigation of evaporation from bare
719 soil under different boundary and initial conditions: An evaluation of nonequilibrium phase
720 change, Water Resour. Res., 51, 7630–7648, doi:10.1002/2014WR016504.
721 van Genuchten MT. 1980. A closed-form equation for predicting the hydraulic conductivity on
722 unsatured soils. Soil Science Society of America Proceedings, 44(5): 892-898.
723 Vásquez C, Ortiz C, Suárez F, Muñoz JF. 2013. Modeling flow and reactive transport to explain
724 mineral zoning in the Atacama salt flat aquifer, Chile. Journal of Hydrology, 490:114-125.
725 Weisbrod N, Nachshon U, Dragila M, Grader A. 2014. Micro-CT analysis to explore salt
726 precipitation impact on porous media permeability. Transport and Reactivity of Solutions in
727 Confined Hydrosystems. Part of the series NATO Science for Peace and Security Series C:
728 Environmental Security, 231-241.
729 Wissmeier L, Barry DA. 2008. Reactive transport in unsaturated soil: Comprehensive modeling
730 of the dynamic spatial and temporal mass balance of water and chemical components,
731 Advances in Water Resources, 31, 858–875.
732

733 **Table captions**

734 Table 1: Coefficients and variables used in the SiSPAT model to estimate liquid water and water
735 vapor flows.

736 Table 2: Model parameters, and initial and boundary conditions.

737 Table 3: Model parameters used for the three horizons.

738 Table 4: Model calibration efficiency for soil water content (θ) and temperature (T), and
739 comparison of the experimental cumulative evaporation and the data obtained from the calibrated
740 model.

741

Author-produced version of the article published in Hydrological Processes (2016), 30 25: 4704-4719
The original publication is available at http://onlinelibrary.wiley.com doi:10.1002/hyp.10987

Figure captions

Figure 1: Observed and modeled soil water content (θ) and temperature profiles, and observed electrical conductivity (σ) profile for different water table levels (WTL), after 20 days of fixing the water table level. Model results assume a vertically homogeneous soil profile. (a) and (b) show the soil water content profiles for WTL of 0.75 and 0.40 m, respectively; (c) and (d) show the temperature profiles for WTL of 0.75 and 0.40 m, respectively; and (e) and (f) show the electrical conductivity profiles for WTL of 0.75 and 0.40 m, respectively.

Figure 2: Observed and modeled soil water content (θ) and temperature profiles for different water table levels (WTL), after 20 days of fixing the water table level and assuming the soil stratifies in three horizons (H1, H2, and H3) due to salt transport. (a) and (b) show the soil water content profiles for WTL of 0.75 and 0.40 m, respectively; (c) and (d) show the temperature profiles for WTL of 0.75 and 0.40 m, respectively.

Figure 3: Variation of liquid and water vapor flux along the soil profile for different water table levels (WTL). (a) and (b) show the liquid flux (q_L), the water vapor flux (q_v) and the total water flux (q_{total}) for WTL of 0.75 and 0.40 m, respectively; (c) and (d) show the thermal vapor flux (q_{vT}), the isothermal (due to pressure) vapor flux (q_{vh}), and the total vapor flux (q_v) for WTL of 0.75 and 0.40 m, respectively. Negative (positive) fluxes correspond to upward (downward) movement.

Author-produced version of the article published in Hydrological Processes (2016), 30 25: 4704-4719
The original publication is available at http://onlinelibrary.wiley.com doi:10.1002/hyp.10987

761 Figure 4: Comparison of cumulative evaporation (mm) for different tortuosity values (τ_a) and
762 enhancement factors (η) for the 0.75 and 0.40-m water table levels. τ_{a*} was calculated based on
763 equation (15) (Millington and Quirk, 1961), and equation (16) was used when η = variable (Cass
764 et al., 1984).

765 Figure 5: Water retention curves fitted for each horizon (H1, H2, and H3) for the 0.75 m water
766 table level (a), and the 0.40 m water table level (b).

767 Figure 6. Comparison of the soil water content and temperature profiles for the 0.75-m (a and c)
768 and 0.40-m (b and d) water table levels (WTL), for the simulation presented in Figure 2 (black)
769 and after steady state was reached (red) when using the bottom boundary conditions equal to the
770 top evaporation flux.

771 Figure 7: Comparison of the water vapor fluxes profiles for the 0.75 and 0.40 m water table levels
772 (WTL). Results are shown for different tortuosity values, τ_a, (a) and (c), and for different
773 enhancement factor values, η (b) and (d). τ_{a*} was calculated based on equation (15) (Millington
774 and Quirk, 1961), and equation (16) was used when η = variable (Cass et al., 1984). Negative
775 (positive) fluxes correspond to upward (downward) movement.

776

Author-produced version of the article published in Hydrological Processes (2016), 30 25: 4704-4719
The original publication is available at http://onlinelibrary.wiley.com doi:10.1002/hyp.10987

777 Table 1: Coefficients and variables used in the SiSPAT model to estimate liquid water and water vapor flows.

778

Parameter	Formula
Saturated vapor pressure	$e_{sat}(T) = 618.78\exp\left(\frac{17.27(T-273.15)}{T-35.86}\right)$
Relative Humidity	$h_u = \exp\left(\frac{h\,g}{RT}\right)$
Vapor density	$\rho_v = \frac{h_u e_{sat}(T)}{RT}$
Diffusivity of water vapor in the air (Philip and De Vries, 1957)	$D_a = 2.17\times10^{-5}\left(\frac{T}{273.15}\right)^{1.88}$
Isothermal diffusivity of water vapor (Philip and De Vries, 1957)	$D_{vh} = \tau_a\, F(\varepsilon-\theta) D_a \frac{P_{atm}}{P_{atm}-e_v}\frac{\partial\rho_v}{\partial h}$
Thermal diffusivity of water vapor (Philip and De Vries, 1957)	$D_{vT} = \eta\, F(\varepsilon-\theta) D_a \frac{P_{atm}}{P_{atm}-e_v}\frac{\partial\rho_v}{\partial T}$
Apparent thermal conductivity (Laurent and Guerre-Chaley, 1995)	$\lambda = \lambda_0 + a_{LG}\frac{\theta}{\theta_S} + b_{LG}\left(1-\exp\left\{-c_{LG}\left(\frac{\theta}{\theta_S}\right)^{d_{LG}}\right\}\right)$

779 θ: volumetric water content ($m^3\ m^{-3}$); θ_s: saturated volumetric water content ($m^3\ m^{-3}$); θ_r: residual
780 volumetric water content ($m^3\ m^{-3}$); α: inverse of the air-entry pressure (m^{-1}); h: water suction (m); n and m
781 are empirical fitting parameters of the water retention curve; K_s: saturated hydraulic conductivity ($m\ s^{-1}$);
782 T: temperature (K); g: gravitational acceleration ($m\ s^{-2}$); R: universal gas constant ($J\ kg^{-1}$); τ_a: soil
783 tortuosity (-); λ_0: dry thermal conductivity; P_{atm}: atmospheric pressure (Pa); e_v: partial pressure of water
784 vapor (Pa); η: enhancement factor (= 1.5); and a_{LG}, b_{LG}, c_{LG}, and d_{LG} are empirical fitting parameters of the
785 Laurent Guerre-Chaley model.
786

Author-produced version of the article published in Hydrological Processes (2016), 30 25: 4704-4719
The original publication is available at http://onlinelibrary.wiley.com doi:10.1002/hyp.10987

787 Table 2: Model parameters and initial and boundary conditions.

Parameter	Value	Observations
Saturated moisture content θ_s ($m^3\ m^{-3}$)	0.3	Measured
Residual moisture content θ_r ($m^3\ m^{-3}$)	0.0	Parameter fitted from the water retention data
Inverse of the air-entry pressure α (m^{-1})	0.7160	Parameter fitted from the water retention data
n (-)	1.1859	Parameter fitted from the water retention data
Saturated hydraulic conductivity K_s ($m\ s^{-1}$)	1.06×10^{-5}	Measured
Porosity (-)	0.3	Assumed equal to the saturated moisture content
a_{LG}	0.3	
b_{LG}	0.5	
c_{LG}	1.0	Parameters of the apparent thermal conductivity from the Laurent and Guerre-Chaley model (1995).
d_{LG}	4.0	
λ_0	0.12	
Initial soil temperature conditions	*T(z)*	Linear interpolation of temperature measurements in the soil at 0.05, 0.10, 0.15, 0.20, 0.25, 0.30, 0.35, 0.40 and 0.45 m. The initial time corresponds to the 1st day after fixing the water table depth.
Initial soil pressure conditions	*h(z)*	Determined from moisture content measurements at 0.05, 0.10, 0.15, 0.20, 0.25, 0.30, 0.35, 0.40 and 0.45 m depth using the water retention curve. The initial time corresponds to the 1st day after fixing the water table depth.
Boundary conditions at the bottom	Known flux	A known water flux equal to the evaporation flux This boundary condition was then evaluated in a sensitivity analysis.
	T(t)	Extrapolated from the measurements of the thermal profile within the soil column.
Boundary condition on the surface	*T(t)*	Temperature measured at the soil column surface.

788

789

Author-produced version of the article published in Hydrological Processes (2016), 30 25: 4704-4719
The original publication is available at http://onlinelibrary.wiley.com doi:10.1002/hyp.10987

790 Table 3: Model parameters used for the three horizons.

Depth of the water table (m)	0.75			0.40		
Horizon	H1	H2	H3	H1	H2	H3
Horizon depth (m)	0.20	0.10	0.90	0.15	0.15	0.90
Saturated moisture content, θ_s (m^3 m^{-3})	0.300	0.300	0.300	0.300	0.300	0.300
Residual moisture content, θ_r (m^3 m^{-3})	0.033	0.000	0.000	0.033	0.000	0.000
Inverse of the air entry pressure, α (cm^{-1})	0.6677	0.7163	0.6667	0.40	0.555	0.6667
Shape parameter of the water retention curve, n (-)	1.2370	1.16	1.2470	1.2370	1.1859	1.2470
Saturated hydraulic conductivity, K_s (m s^{-1})	$1.5x10^{-5}$	$5.0x10^{-5}$	$1.0x10^{-5}$	$1.0x10^{-8}$	$1.5x10^{-8}$	$1.0x10^{-5}$
Shape factor of the hydraulic conductivity curve, β (-)	18	18	18	25	30	30
a_{LG}	0.300			0.734		
b_{LG}	0.9			0.3		
c_{LG}	35.0			35.0		
d_{LG}	5.00			3.82		
λ_0	0.12			0.50		

791
792
793
794
795
796

Author-produced version of the article published in Hydrological Processes (2016), 30 25: 4704-4719
The original publication is available at http://onlinelibrary.wiley.com doi:10.1002/hyp.10987

797 Table 4: Model calibration efficiency for soil water content (θ) and temperature (T), and comparison of the
798 experimental cumulative evaporation and the data obtained from the calibrated model.
799

	Depth to groundwater table (m)	
	0.75	0.40
$RMSE_\theta$ (m^3 m^{-3})	0.0095	0.020
B_θ (m^3 m^{-3})	0.002	-0.0003
E_θ (-)	0.985	0.50
$RMSE_T$ (°C)	2.08	2.61
B_T (°C)	0.40	-2.41
E_T (-)	0.67	0.46
Experimental cumulative evaporation (mm)	0.85	5.78
Modeled cumulative evaporation (mm)	0.86	5.11

800 *RMSE*: root mean square error; *B*: bias; *E*: Nash-Sutcliffe efficiency
801

802

Author-produced version of the article published in Hydrological Processes (2016), 30 25: 4704-4719
The original publication is available at http://onlinelibrary.wiley.com doi:10.1002/hyp.10987

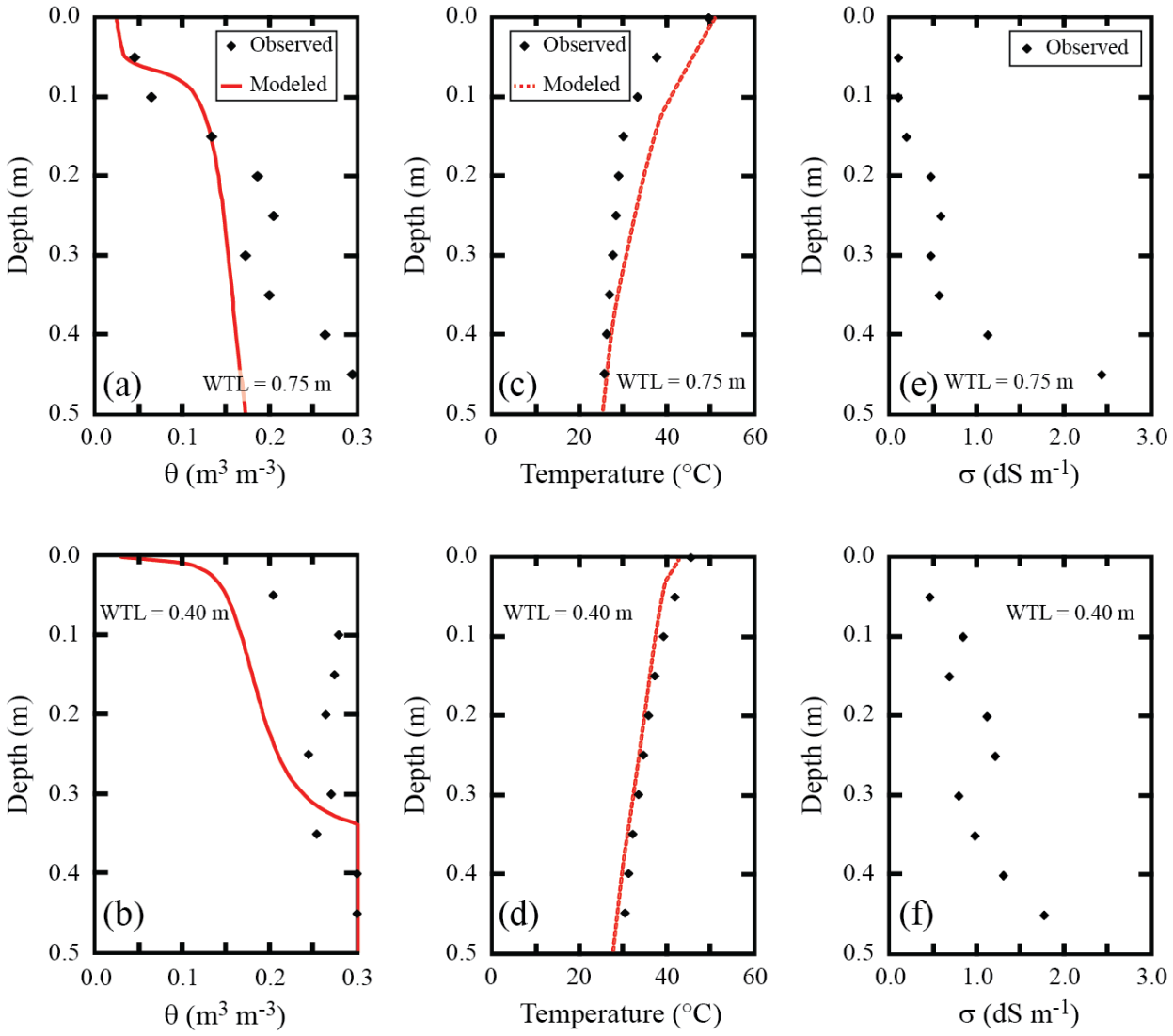

Figure 1: Observed and modeled soil water content (θ) and temperature profiles, and observed electrical conductivity (σ) profile for different water table levels (WTL), after 20 days of fixing the water table level. Model results assume a vertically homogeneous soil profile. (a) and (b) show the soil water content profiles for WTL of 0.75 and 0.40 m, respectively; (c) and (d) show the temperature profiles for WTL of 0.75 and 0.40 m, respectively; and (e) and (f) show the electrical conductivity profiles for WTL of 0.75 and 0.40 m, respectively.

Author-produced version of the article published in Hydrological Processes (2016), 30 25: 4704-4719
The original publication is available at http://onlinelibrary.wiley.com doi:10.1002/hyp.10987

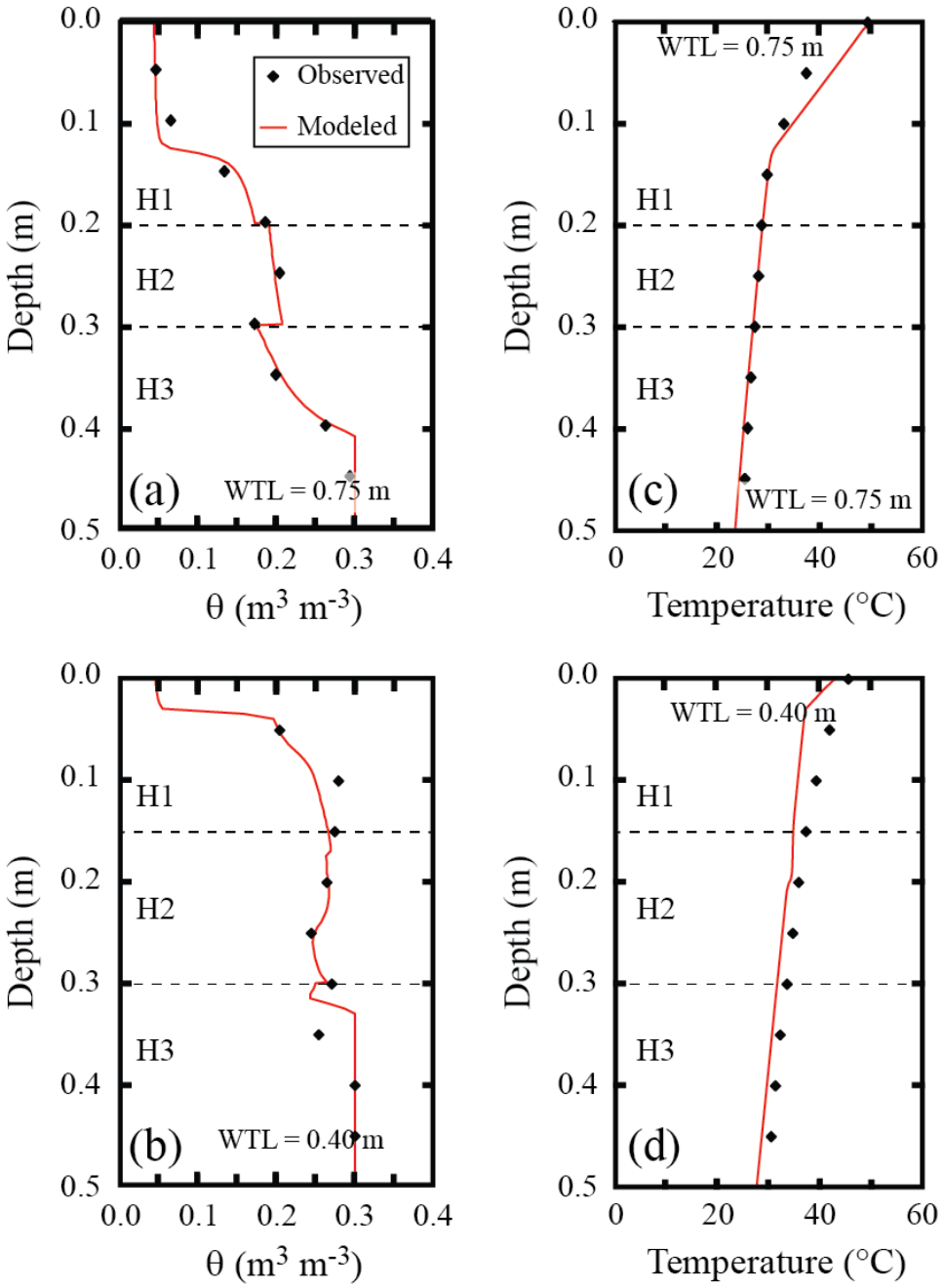

Figure 2: Observed and modeled soil water content (θ) and temperature profiles for different water table levels (WTL), after 20 days of fixing the water table level and assuming the soil stratifies in three horizons (H1, H2, and H3) due to salt transport. (a) and (b) show the soil water content profiles for WTL of 0.75 and 0.40 m, respectively; (c) and (d) show the temperature profiles for WTL of 0.75 and 0.40 m, respectively.

Author-produced version of the article published in Hydrological Processes (2016), 30 25: 4704-4719
The original publication is available at http://onlinelibrary.wiley.com doi:10.1002/hyp.10987

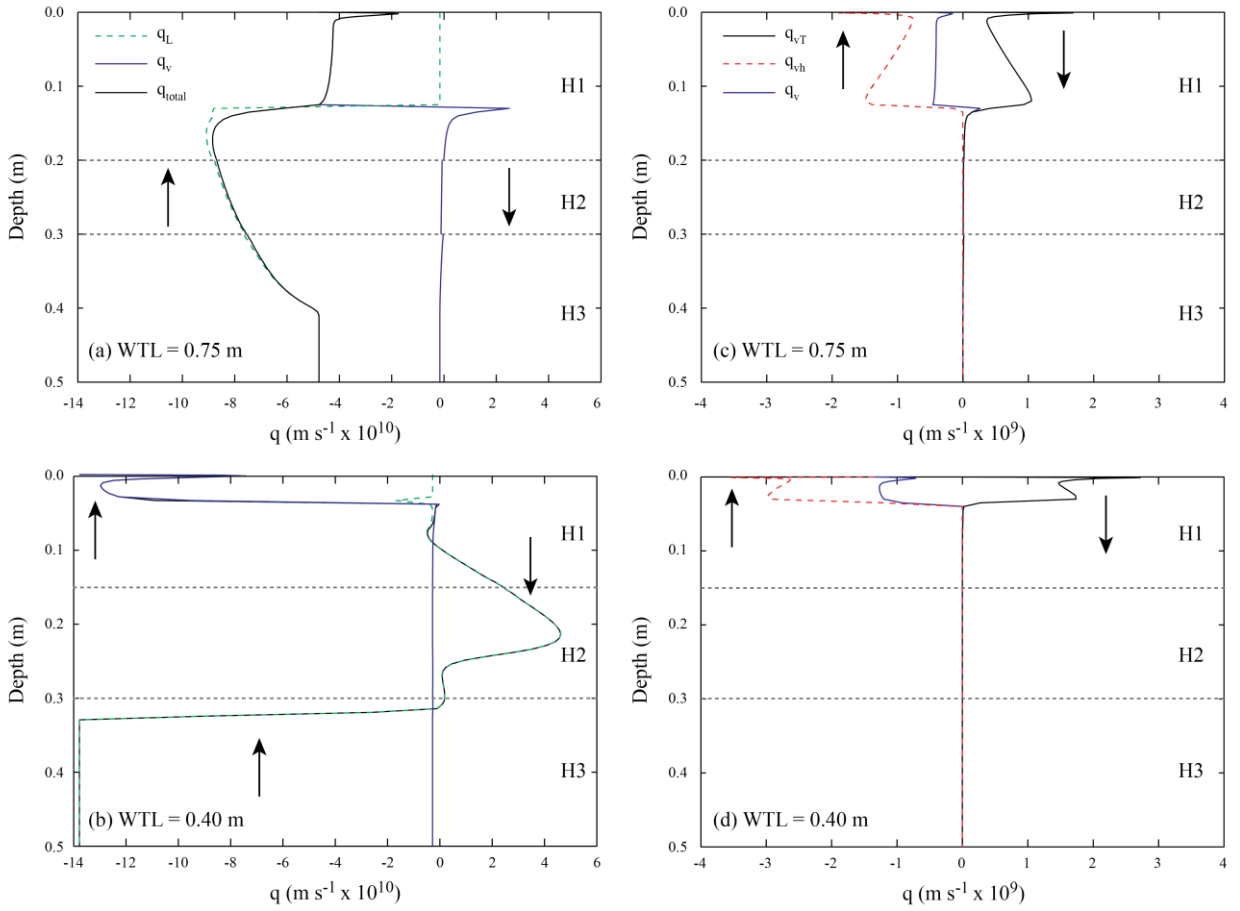

Figure 3: Variation of liquid and water vapor flux along the soil profile for different water table levels (WTL). (a) and (b) show the liquid flux (q_L), the water vapor flux (q_v) and the total water flux (q_{total}) for WTL of 0.75 and 0.40 m, respectively; (c) and (d) show the thermal vapor flux (q_{vT}), the isothermal (due to pressure) vapor flux (q_{vh}), and the total vapor flux (q_v) for WTL of 0.75 and 0.40 m, respectively. Negative (positive) fluxes correspond to upward (downward) movement.

Author-produced version of the article published in Hydrological Processes (2016), 30 25: 4704-4719
The original publication is available at http://onlinelibrary.wiley.com doi:10.1002/hyp.10987

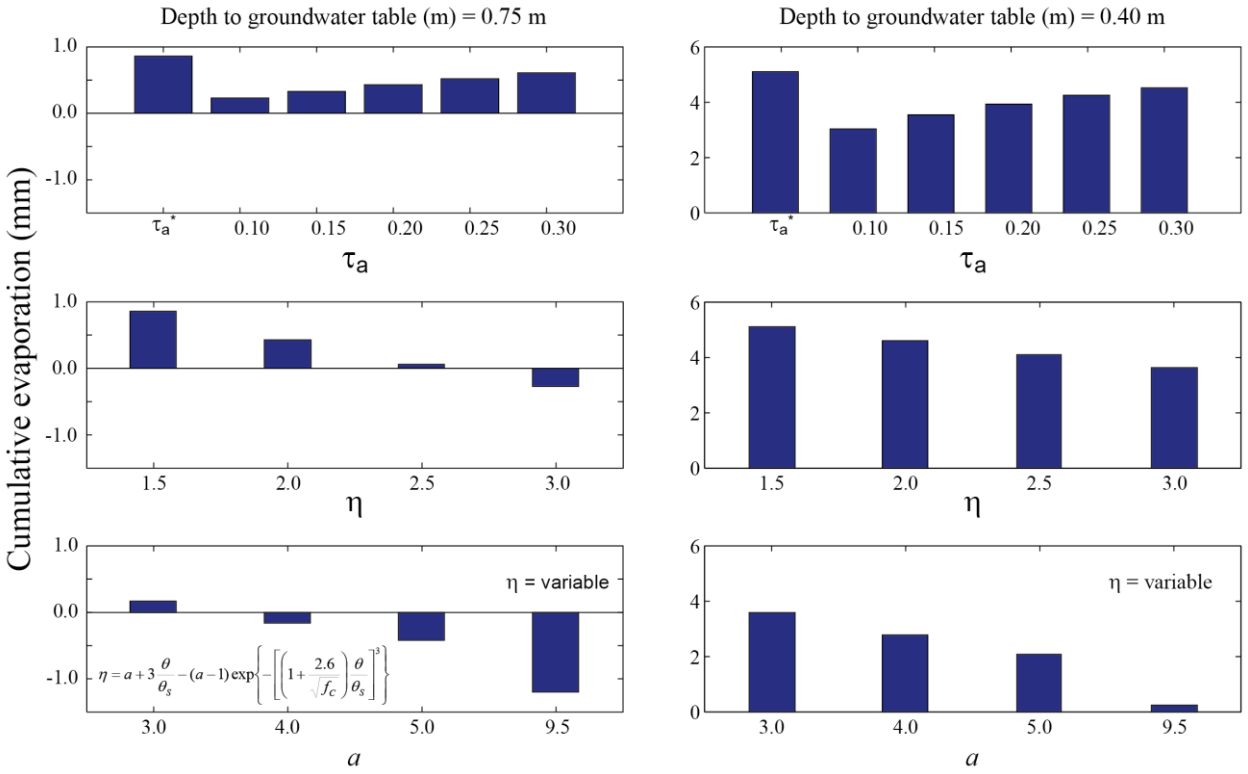

Figure 4: Comparison of cumulative evaporation (mm) for different tortuosity values (τ_a) and enhancement factors (η) for the 0.75 and 0.40-m water table levels. τ_a* was calculated based on equation (15) (Millington and Quirk, 1961), and equation (16) was used when η = variable (Cass et al., 1984).

Author-produced version of the article published in Hydrological Processes (2016), 30 25: 4704-4719
The original publication is available at http://onlinelibrary.wiley.com doi:10.1002/hyp.10987

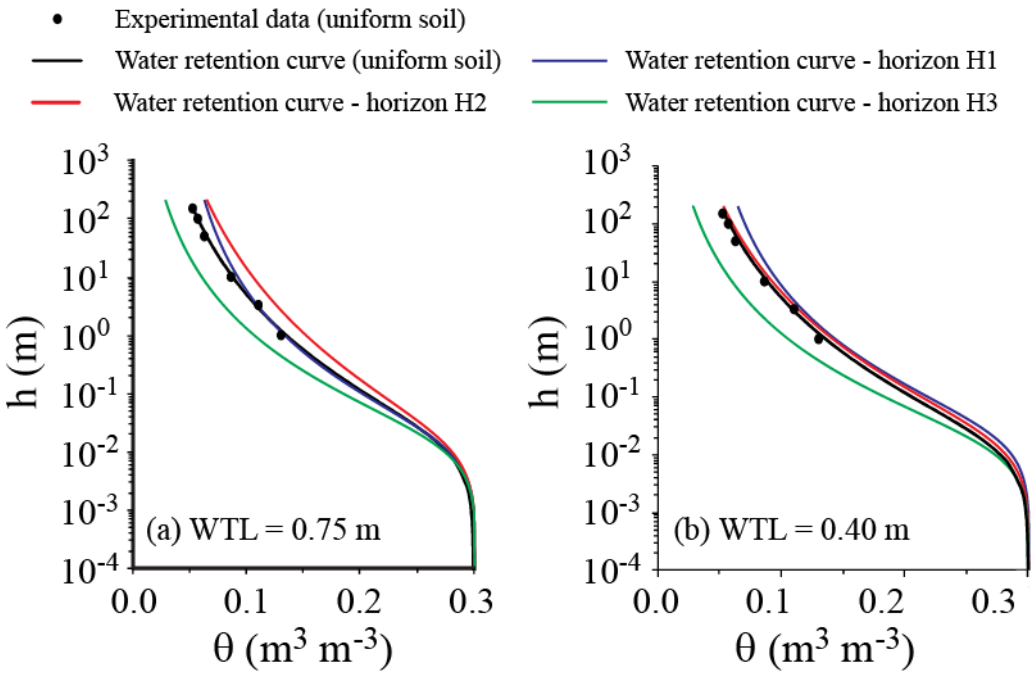

828

829 Figure 5: Water retention curves fitted for each horizon (H1, H2, and H3) for the 0.75 m water table level (a), and the

830 0.40 m water table level (b).

831

832

Author-produced version of the article published in Hydrological Processes (2016), 30 25: 4704-4719
The original publication is available at http://onlinelibrary.wiley.com doi:10.1002/hyp.10987

833

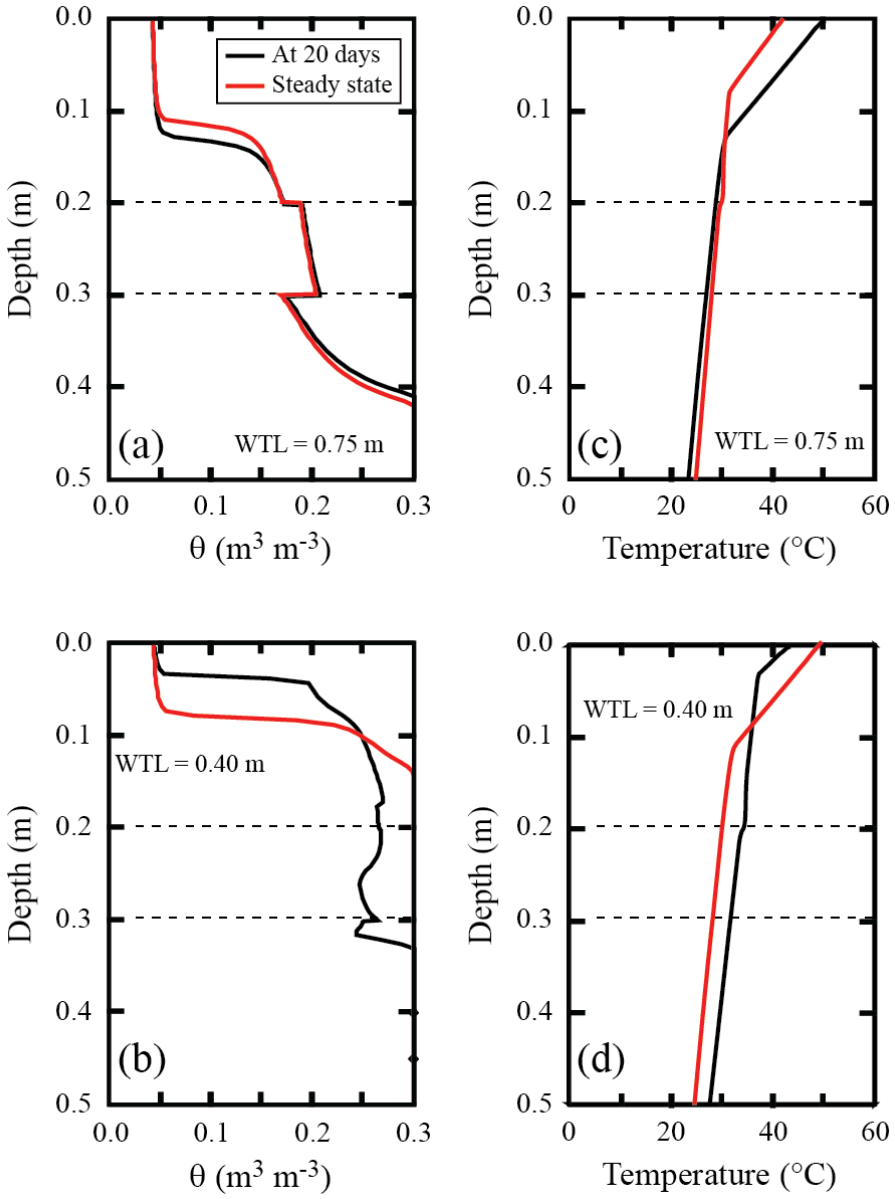

834

835 Figure 6. Comparison of the soil water content and temperature profiles for the 0.75-m (a and c) and 0.40-m (b and
836 d) water table levels (WTL), for the simulation presented in Figure 2 (black) and after steady state was reached (red)
837 when using the bottom boundary conditions equal to the top evaporation flux.

838

Author-produced version of the article published in Hydrological Processes (2016), 30 25: 4704-4719
The original publication is available at http://onlinelibrary.wiley.com doi:10.1002/hyp.10987

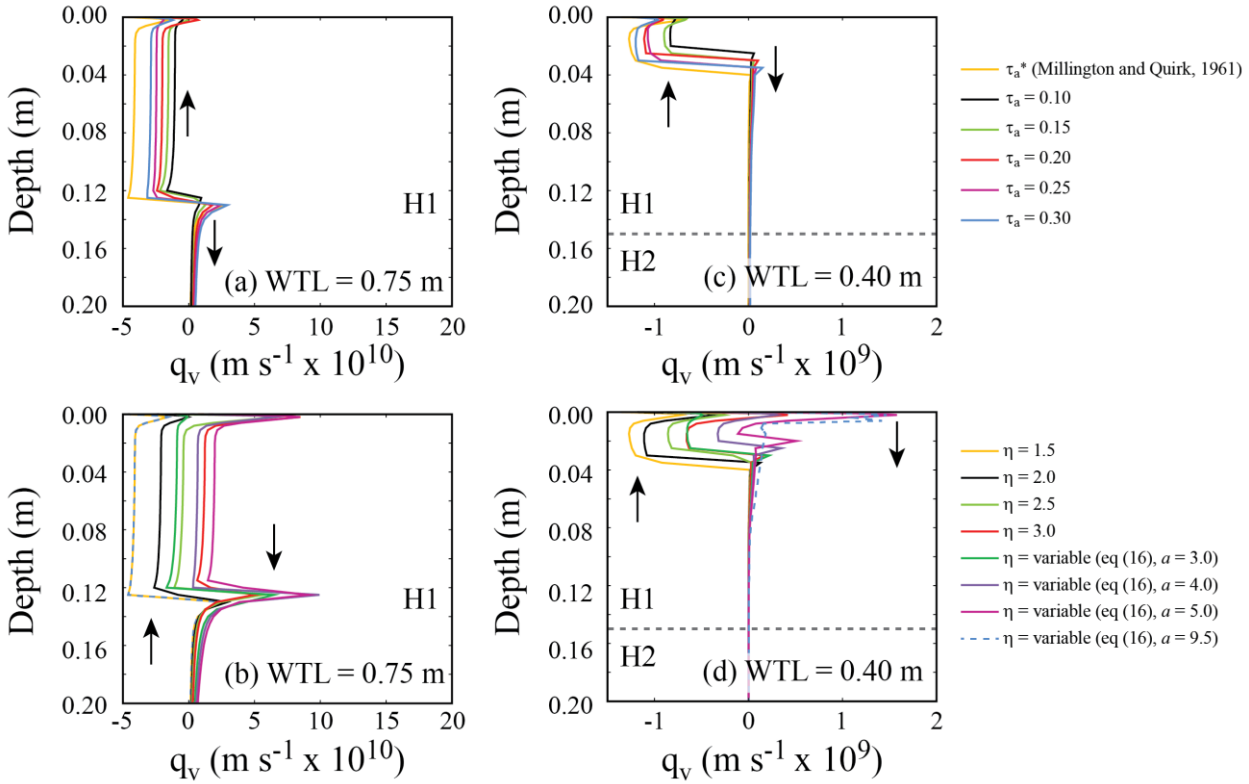

Figure 7: Comparison of the water vapor fluxes profiles for the 0.75 and 0.40 m water table levels (WTL). Results are shown for different tortuosity values, τ_a, (a) and (c), and for different enhancement factor values, η (b) and (d). τ_a* was calculated based on equation (15) (Millington and Quirk, 1961), and equation (16) was used when η = variable (Cass et al., 1984). Negative (positive) fluxes correspond to upward (downward) movement.